Remote Sens. **2013**, *5*, 2704-2719; doi:10.3390/rs5062704

OPEN ACCESS

Remote Sensing

ISSN 2072-4292

www.mdpi.com/journal/remotesensing

Article

Characterization of Landslide Deformations in Three Gorges Area Using Multiple InSAR Data Stacks

Peraya Tantianuparp, Xuguo Shi, Lu Zhang *, Timo Balz and Mingsheng Liao

State Key Laboratory of Information Engineering in Surveying, Mapping and Remote Sensing, Wuhan University, Wuhan 430079, China; E-Mails: java_apple@hotmail.com (P.T.); xuguoshi@whu.edu.cn (X.S.); balz@whu.edu.cn (T.B.); liao@whu.edu.cn (M.L.)

* Author to whom correspondence should be addressed; E-Mail: luzhang@whu.edu.cn; Tel.: +86-27-6877-8395; Fax: +86-27-6877-8229.

Received: 4 April 2013; in revised form: 22 May 2013 / Accepted: 23 May 2013 / Published: 28 May 2013

Abstract: In the areas with steep topography and vulnerable geological condition, landslide deformation monitoring is an important task for risk assessment and management. Differential Synthetic-Aperture Radar interferometry (D-InSAR) and Persistent Scatterer Interferometry (PS-InSAR) are two advanced SAR Interferometry techniques for detection, analysis and monitoring of slow moving landslides. The techniques can be used to identify wide displacement areas and measure displacement rates over long time series with millimeter-level accuracy. In this paper, multiple SAR datasets of Advanced Land Observing Satellite (ALOS) Phased Array L-band Synthetic Aperture Radar (PALSAR) and Environmental Satellite (ENVISAT) C-band Advanced Synthetic Aperture Radar (ASAR) are used for landslide monitoring with both D-InSAR and PS-InSAR techniques in Badong at the Three Gorges area in China. Two areas of significant deformation along the southern riverbank of Yangtze River in Badong are identified by joint analyses of PS-InSAR results from different data stacks. Furthermore, both qualitative and quantitative evaluations of the PS-InSAR results are carried out together with preliminary correlation analysis between the time series deformation of a PS point in high risk location and the temporal variation of water level in the Three Gorges Reservoir.

Keywords: landslide; deformation monitoring; Three Gorges; D-InSAR; PS-InSAR

1. Introduction

Synthetic-Aperture Radar interferometry (InSAR) is a powerful technique that exploits phase information of SAR images to measure ground surface movements. An important application of satellite SAR data acquired in repeat-pass mode is the deformation monitoring using Differential SAR interferometry (D-InSAR) technique with sub-centimeter accuracy [1]. This technique is well-known for its applications in subsidence and landslide monitoring [2,3] as well as seismic analysis [4,5].

However, practical applications of D-InSAR are limited by major drawbacks such as geometric and temporal decorrelation, as well as atmospheric disturbances [6]. With the Persistent Scatterers SAR Interferometry (PS-InSAR) techniques, a long time series of SAR images is combined to identify point-like stable reflectors (PSs), which can overcome the problems for traditional D-InSAR technique so as to improve the accuracy and reliability of deformation measurements [7]. PS-InSAR has been widely applied in urban land subsidence across the world in the past decade, and millimeter-level deformation measurement accuracy can often be achieved [6,8]. However, its application in landslide deformation monitoring has just become a hot topic of research in recent years [9–11]. Landslide monitoring in the Three Gorges areas with InSAR techniques is difficult due to environmental conditions such as strong terrain relief, dense vegetation cover, and complicated atmospheric variation [12]. Such problems may hinder the PS-InSAR analysis. To solve such problems, Hooper developed the Stanford Method for Persistent Scatterers (StaMPS) to make use of spatial-temporal filtering to extract deformation components from time-series interferometric phase signal [13].

The ongoing operation of satellite SAR systems and new SAR satellite development have accumulated large volumes of archived SAR datasets, with which appropriate integrated analyses of multi-frequency, multi-resolution, and multi-track SAR datasets are possible. Multiple-platform SAR observations of the same area from different orbits have been used to improve the extraction of topographic and displacement information [14].

In this paper, we investigated the application of D-InSAR and PS-InSAR techniques in landslide movement detection and analysis at Badong in the Three Gorges area. Both L-band Advanced Land Observing Satellite (ALOS) Phased Array L-band Synthetic Aperture (PALSAR) and C-band Environmental Satellite (ENVISAT) Advanced Synthetic Aperture Radar (ASAR) datasets of multiple tracks acquired during the last five years are used as test data. Using PS-InSAR method, we can identify areas with high risks of slope failure in Badong and detect time-series deformation at landslide bodies. The results from the three tracks are converted from displacement along the line of sight (LOS) direction into down-slope movement to facilitate inter-stack comparison. The comparison shows good consistency among the results in the identification of the Huangtupo landslide near the old town of Badong.

2. Study Area and Test Datasets

2.1. Study Area

As the largest hydro-electric project in the world, the Three Gorges Project (TGP) was fully functional in 2009. With the operation of the huge dam at Sandouping, the water level in the Three Gorges Reservoir rose to 175 m above sea level for the first time in 2010. Nowadays, the reservoir water level fluctuates between 145 m and 175 m bi-annually during each storage-discharge cycle. Such

a big and frequent variation will inevitably affect slope stability along the Yangtze River and its tributaries in the Three Gorges Region, including reactivation of some old landslides and triggering new slope failures. Therefore, landslide monitoring will always be a task of major concern in the post-TGP era [15].

Badong, an ancient city located between Wu Gorge and Xiling Gorge along Yangtze River, is taken as our study area. The old town has been demolished and submerged due to water level rise along with the TGP construction. The new town of Badong is relocated upriver, *i.e.*, to the west of the old town. Geographic locations of Badong as well as the Three Gorges Dam are shown in Figure 1(a).

Figure 1. (**a**) Location map of the study area (**b**) Geological map of Badong County (adapted from [16]).

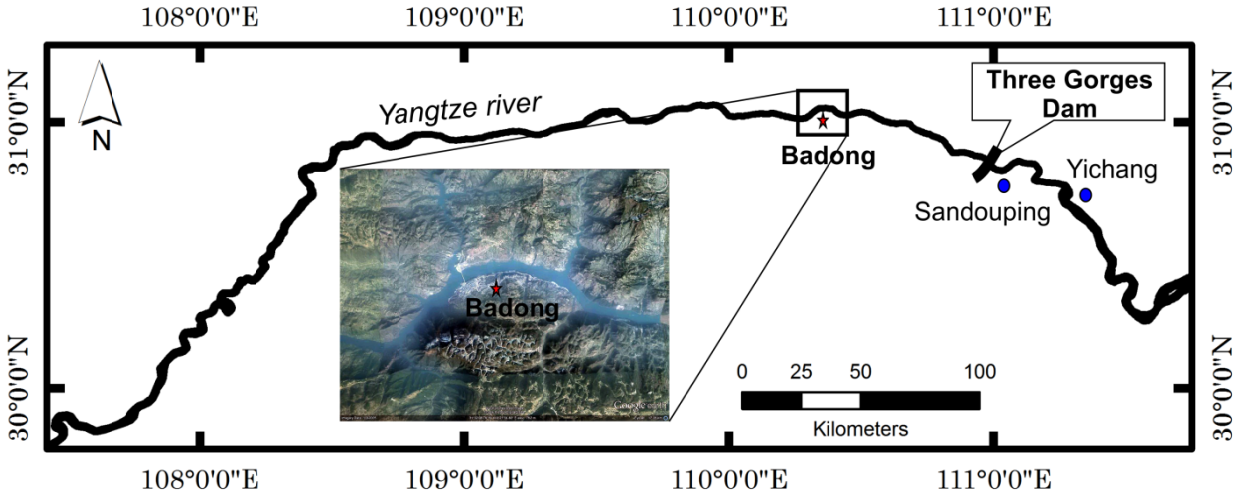

(**a**)

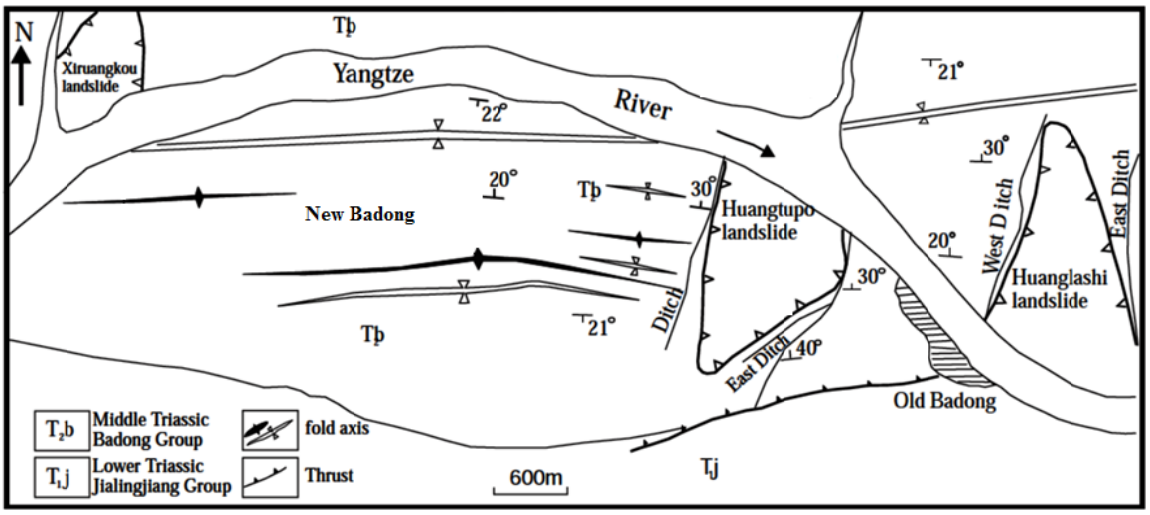

(**b**)

Because the new Badong town was built along a steep river bank, the impact of water-level variation in the Three Gorges reservoir is of great concern. Furthermore, slope instability in Badong is induced by various kinds of triggering factors, such as rainfall, human activity, and geological environment change. Geological setting of the Badong area is shown in Figure 1(b). The basement rock type in Badong consists of two main groups, *i.e.*, the middle Triassic Badong group (T_2b) and the lower

Triassic Jialingjiang group (T_1J). The rock members of middle Triassic Badong group located in the Badong new city near the Yangtze River are pelitic siltstone and pelitic limestone. The rock type in the lower Triassic Jialingjiang group is limestone situated in the upper part of the slope. Its landscape indicates that one of the most significant geomorphological characteristic is the strata dip toward the bank of the Yangtze River. Buildings located on this slope are affected by potential slope instability [17].

In order to monitor slope surface movements in the Badong area, many investigators have used different instruments and methods. For examples, landslide hazard assessments have been carried out in the Three Gorges area of Yangtze River using ASTER imagery [18], using D-InSAR with corner reflectors [19], and also using PS-InSAR technique [12,20].

2.2. Test Datasets

In our experiments, we use three InSAR time-series data stacks covering the same area to detect landslide deformation in the Badong area. We use one stack of L-band ALOS PALSAR data and two stacks of C-band ENVISAT ASAR data.

2.2.1. Advanced Land Observing Satellite (ALOS) Phased Array L-band Synthetic Aperture (PALSAR)

A stack of 22 images acquired by the ALOS PALSAR system from an ascending orbit during the period from December 2006 to February 2011 was provided by JAXA. All these SAR images are L1.0 products. The data stack consists of both single-polarization (FBS) and dual-polarization (FBD) mode images. The largest temporal baseline is 1,150 days and the normal baseline ranges from 155 m to 2,443 m. The stack covers an area of about 326 km^2.

2.2.2. Environmental Satellite (ENVISAT) Advanced Synthetic Aperture Radar (ASAR)

Two time-series of ENVISAT ASAR data acquired from different orbit directions (one ascending and one descending) are provided by ESA. The ascending stack of 17 images was acquired between February 2006 and February 2010. The largest temporal baseline is 1,190 days and the normal baseline varies between 18 m and 867 m. It covers an area of 352 km^2. The descending stack consists of 21 images collected from March 2008 to August 2010. The corresponding largest temporal baseline is 455 days and the normal baseline ranges from 21 m to 270 m. The area of the descending stack is 440 km^2.

3. Synthetic-Aperture Radar (SAR) Interferometry for Landslide Analysis

In this study, both D-InSAR and PS-InSAR techniques will be used to measure landslide surface motion in Badong County.

3.1. Differential Synthetic-Aperture Radar Interferometry (D-InSAR)

D-InSAR data processing can be implemented in several ways. Most commonly used is the two-pass method, which uses two SAR images for interferogram generation and then removes the topographic phase estimated from an existing digital elevation model (DEM).

Theoretically, D-InSAR can detect millimeter-level deformation. However, its performance for landslide monitoring application is reduced due to the loss of coherence between the two observations

as well as atmospheric phase screen. Furthermore, other factors may degrade the quality of differential interferograms, such as the DEM error or the error in image co-registration.

3.2. Persistent Scatterer Interferometry (PS-InSAR)

Persistent Scatterer Interferometry (PS-InSAR) is an advanced technique to derive information of terrain motion [7]. PS-InSAR can overcome the limitations of geometrical and temporal decorrelation as well as atmospheric disturbance. This technique uses multiple SAR acquisitions of the same area to build a stack of interferograms, from which point-like stable reflectors, *i.e.*, the so-called persistent scatterers (PS), are identified. The coherent measurements on PSs allow a terrain movement estimation with sub-millimeter accuracy [21].

In our study, the Delft object-oriented radar interferometric software (Doris) was used for Interferometric SAR processing. Because the Doris Software only support Single Look Complex format (SLC) data, we used the Repeat Orbit Interferometry PACkage (ROI_PAC) for focusing RAW datasets of ALOS PALSAR into SLC format to be ingested into Doris. After the interferogram formation, we used the Stanford Method for Persistent Scatterers (StaMPS) to identify PS points and estimate the displacements at these points.

4. Experimental Results and Analyses

4.1. Differential Synthetic-Aperture Radar Interferometry (D-InSAR)

4.1.1. Analysis of Coherence Images

Coherence, an indicator of InSAR data quality, is estimated from the complex cross-correlation coefficient of the SAR image pair. We examine two interferometric pairs from each InSAR data stack for our comparison, *i.e.*, one short and one long time interval pair. Evaluation of coherence measurements from the three stacks indicates that the overall coherence is higher for the data pairs with short time intervals and relatively small normal baselines. Meanwhile, the coherence is relatively low for data pair of long time interval in all stacks. All results are shown in Figure 2 and the information of each interferogram is listed in Table 1.

Table 1. The interferogram information for coherence analysis.

Pair	SAR Sensor	Orbit Direction	Date		Normal Baseline (m)	Temporal Baseline (day)
			Master	Slave		
a	ALOS PALSAR	ascending	2007/12/30	2010/02/19	156	782
b			2007/12/30	2011/02/22	1,868	1,150
c	ENVISAT ASAR	ascending	2009/05/16	2009/11/07	47	175
d			2009/05/16	2006/07/01	−795	−1,050
e		descending	2009/05/17	2009/07/26	−97	70
f			2009/05/17	2009/11/08	270	175

Figure 2. Coherence images associated with the interferograms from the six Synthetic-Aperture Radar Interferometry (InSAR) data pairs listed in Table 1.

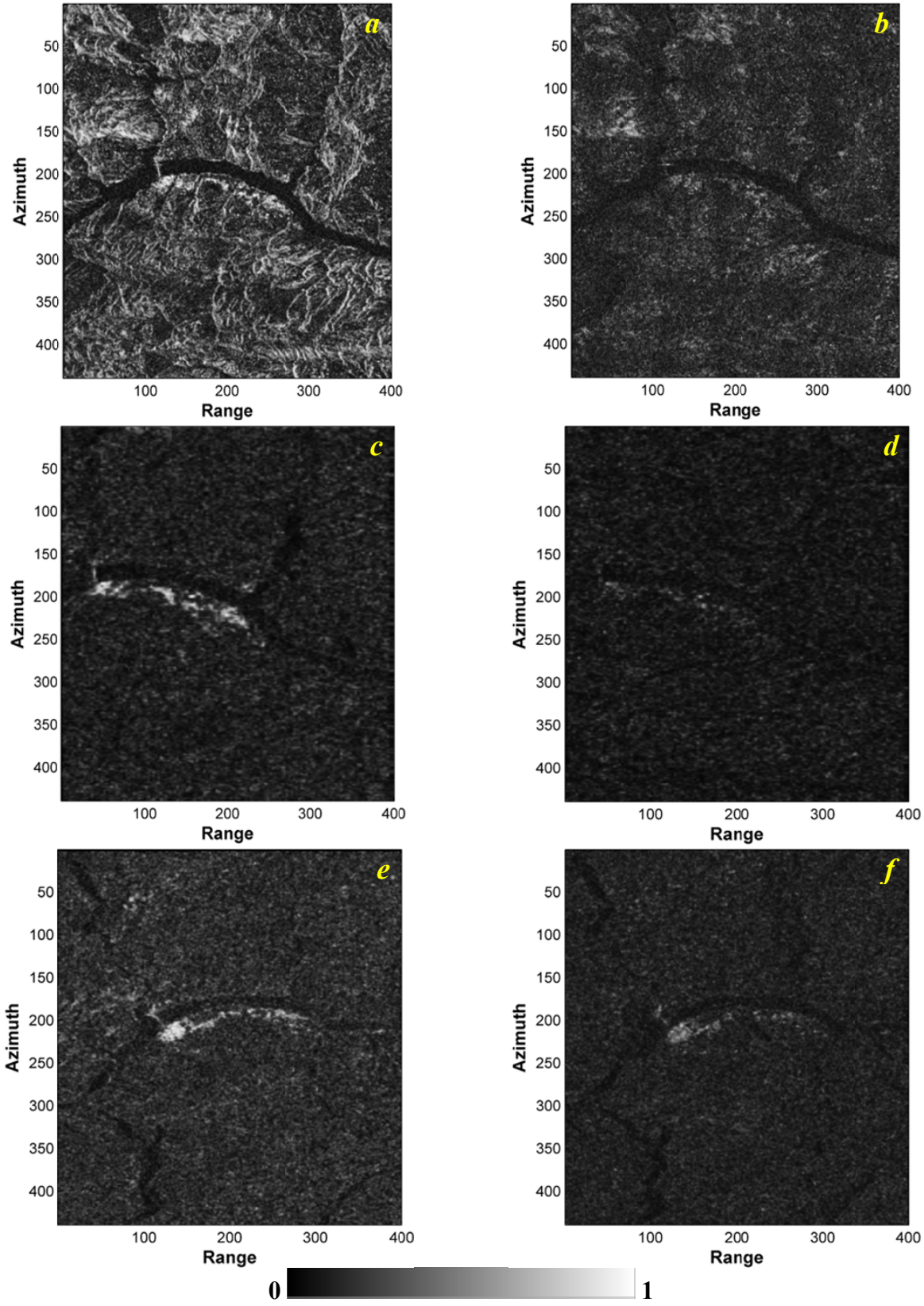

4.1.2. Analysis of Interferograms

The interferometric phase is produced from phase difference calculation between two SAR images pixel by pixel. It is useful for analyzing wide-area terrain movements in the LOS direction. After removing the topographic phase from the interferograms, fringes should only show up at areas with a high deformation rate. Location of landslide deformation in the large scale can be roughly identified by analysis of fringe density in differential interferograms. From Figure 3 we can see that all differential interferograms with small normal baselines can show the Huangtupo landslide, a large landslide located on the southern riverbank of the Yangtze River. Meanwhile, other differential interferograms with long normal baselines are not good enough for identifying landslide deformations. The white squares in Figure 3 show the deformation area of this landslide that appears in interferograms of ALOS PALSAR and ENVISAT ASAR datasets with small normal baselines (156 m, 47 m and 97 m), respectively. However, D-InSAR in the Three Gorges region does not only suffer from the strong temporal decorrelation, but also from the lack of good external DEMs, which causes several fringes in the differential interferogram which could be misinterpreted as surface motions [22].

Figure 3. Differential interferograms after removal of topographic phase. (**a**) Interferogram of Advanced Land Observing Satellite (ALOS) Phased Array L-band Synthetic Aperture Radar (PALSAR) data pair (2007/12/30 *vs.* 2010/02/19, B_n = 156 m), (**b**) Interferogram of ascending Environmental Satellite (ENVISAT) Advanced Synthetic Aperture Radar (ASAR) data pair (2009/05/16 *vs.* 2009/11/07, B_n = 47 m) and (**c**) Interferogram of descending ENVISAT ASAR data pair (2009/05/17 *vs.* 2009/07/26, B_n = 97 m). The white square indicates the location of Huangtupo landslide.

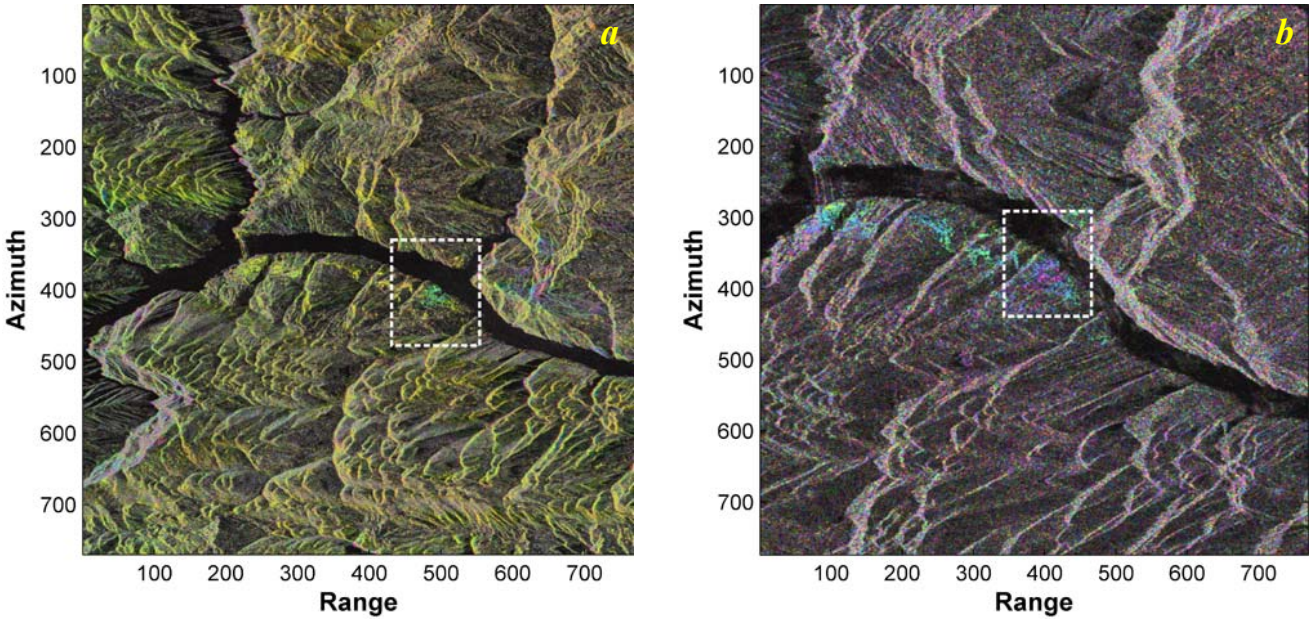

Figure 3. *Cont.*

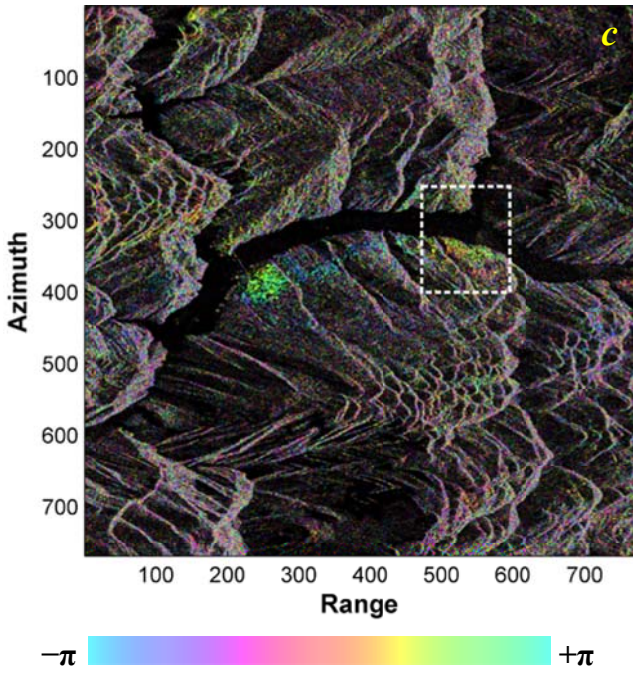

4.2. Persistent Scatterer Interferometry (PS-InSAR) Analysis

4.2.1. Qualitative Evaluation of Persistent Scatterer (PS) Distributions from Different Synthetic-Aperture Radar interferometry (InSAR) Data Stacks

All of the three data stacks (one ALOS PALSAR and two ENVISAT ASAR datasets) cover both the old town and the new town of Badong, but they are not exactly identical to each other. As the system configurations for the three data stacks are quite dissimilar, differences in the spatial distribution patterns of PS points from the three data stacks are expected. Figure 4 shows the spatial distribution of PS points identified from the three stacks. The PS point density of the ALOS PALSAR dataset is quite high and distributed evenly across the area. By contrast, in the results of the two ENVISAT ASAR stacks, dense PS points can be detected only along the southern riverbank and the distribution of PS points is sparse in other areas. Such differences could be explained by the fact that L-band SAR has a better capability of penetrating vegetation canopy than C-band. As a result, much more stable reflectors might be observed in the Three Gorges area using L-band. Therefore, from the perspective of achieving high density of PS points in rural areas like the Three Gorges, it is more preferable to use L-band SAR data rather than C-band data. In this study we select a PS point located at the square besides the county council building as the reference point for comparing the results from the three datasets directly in the next section, the reference point is shown in Figure 4(c).

Figure 4 not only shows the spatial density of the PS points, but also reveals the spatial variability of the mean deformation velocities in each data stack. In Figure 4(a), *i.e.*, the result of the ALOS PALSAR data stack, the most significant deformation is observed at Huangtupo landslide, and slow deformations are detected in the western part near the reference point. The PS LOS displacement rates from the two ENVISAT ASAR stacks show generally a similar behavior. The mean velocities from the ascending stack (Figure 4(b)) could be divided into four subzones along the Yangtze River, *i.e.*, fast

deformation, rather stable, slow deformation, and rather stable from east to west (area 1–4), respectively. The mean velocities from the descending stack (Figure 4(c)) show two fast deformation zones (circled areas) located along the southern riverbank of the Yangtze River. From this comparison, we can see that the spatial variability of the mean deformation velocity for the two ASAR stacks is higher than that of the PALSAR stack. This pattern shows the advantage of C-band SAR data over L-band in sensitivity of deformation measurement when the deformation can be observed in both data stacks.

Figure 4. Deformation velocities at PS points in Badong identified by PS-InSAR: (**a**) from Advanced Land Observing Satellite (ALOS) Phased Array L-band Synthetic Aperture Radar (PALSAR) data; (**b**) from Environmental Satellite (ENVISAT) Advanced Synthetic Aperture Radar (ASAR) ascending data; and (**c**) from ENVISAT ASAR descending data. The numbered circles outline the two active landslides. The number 1 in (a) refers to the Huangtupo landslide. The red lines in (b) divided the southern riverbank into several significant deformation zones. The red star in (c) indicates the location of the reference point.

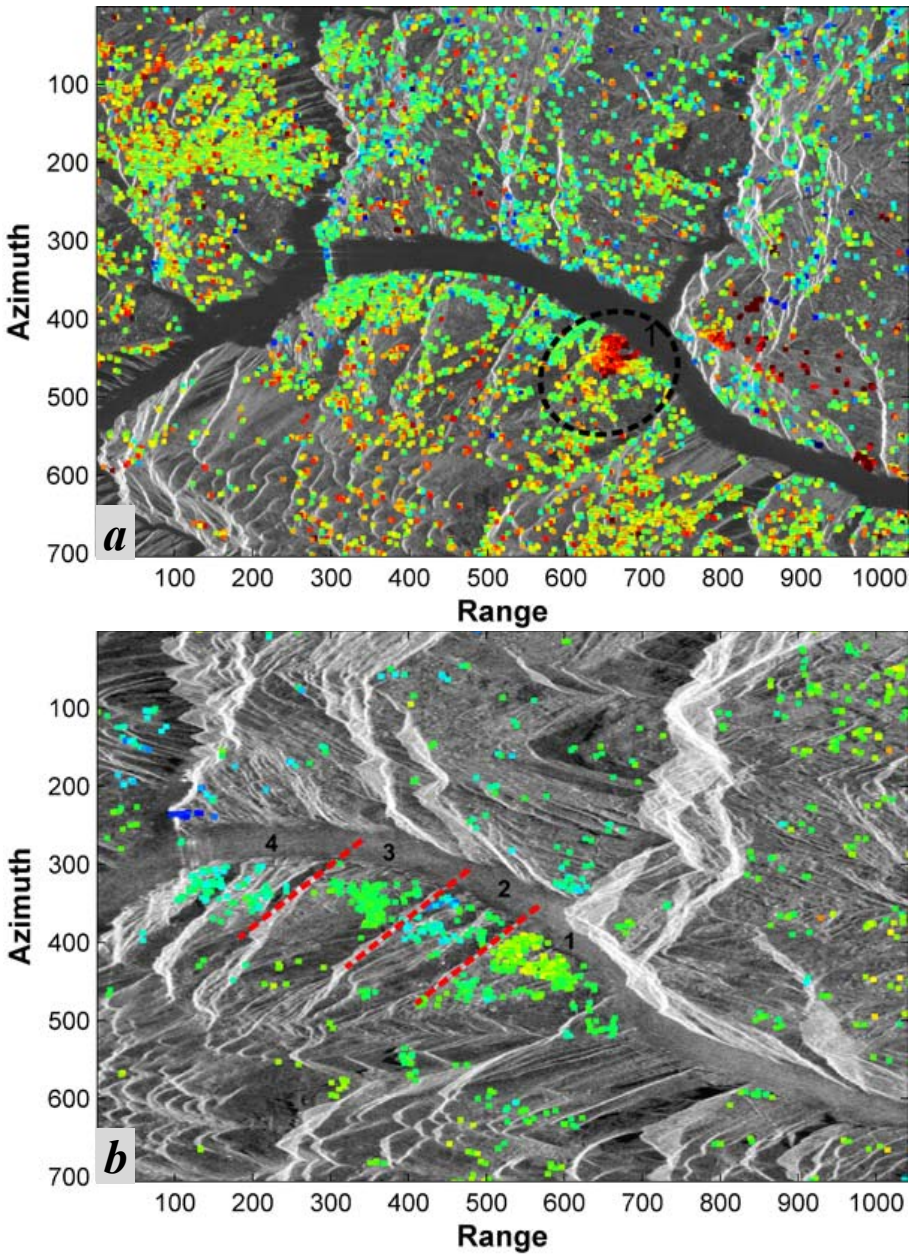

Figure 4. *Cont.*

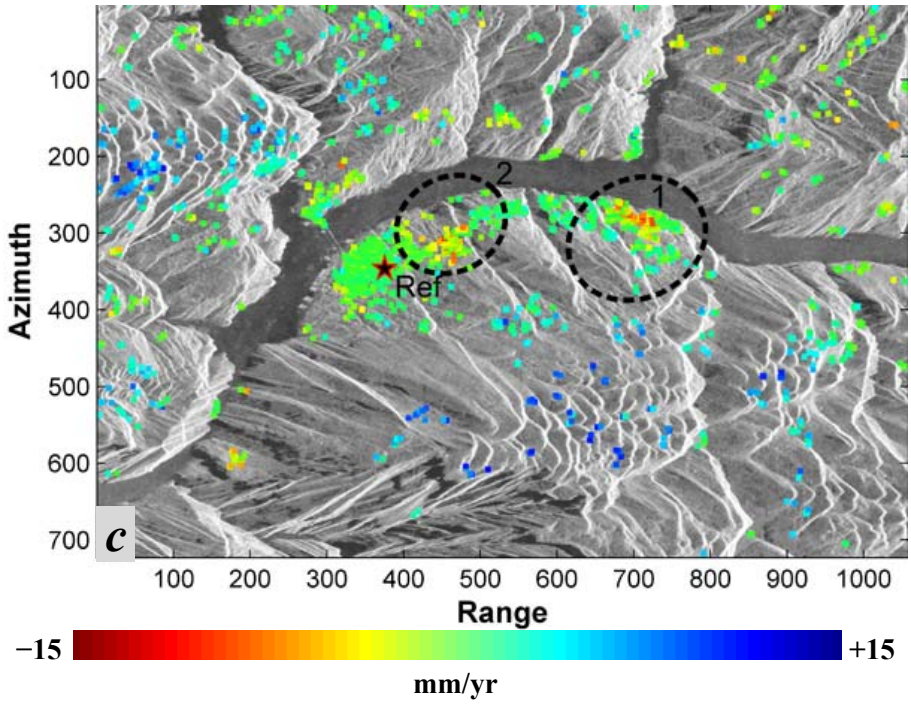

Apart from these two findings, we also notice another interesting phenomenon. Along the southern riverbank of the Yangtze River, two areas of significant deformation are identified in Badong by the two ENVISAT ASAR data stacks acquired from different orbits. PS-InSAR results from both ENVISAT ASAR data stacks show the significant deformation in the eastern part of the area (circle 1), but the fast deformation in the western part (circle 2 in Figure 4(c)) seems to show up only in the result from the descending stack. According to publicly available documents, the eastern area corresponds to the Huangtupo landslide near the old town, while the western one is in the new town of Badong. In the result of L-band PALSAR data stack acquired from an ascending orbit, the deformation in the eastern site is also clearly identified, while the western one is again not detected. By considering the fact that the analysis of using multiple InSAR dataset can only detect displacements in the LOS direction and investigating the topographic characteristics of the area around new Badong city, we infer that it is because the displacement vectors are nearly orthogonal to the LOS vector for the ascending SAR data stacks so that they cannot be detected in the results of ascending stacks. This phenomenon demonstrates that sometimes using just a single InSAR data stack is insufficient to characterize all deformations within a certain region, and it is necessary to carry out joint analyses of multiple stacks of different orbits.

4.2.2. Quantitative Comparison of Mean Deformation Velocities from Different Stacks

Quantitative accuracy assessment of the mean deformation velocity is essential for evaluating the usability and reliability of PS-InSAR in practical applications. However, since no ground-truth data such as leveling or GPS measurements are available in this study area, we can only use an alternative approach, *i.e.*, performing cross-validation among the results from the three InSAR data stacks.

As already mentioned, the deformation velocity measured by the PS-InSAR analysis is merely along the LOS direction. Therefore, the results, *i.e.*, the mean deformation velocities at PS points obtained from different data stacks, could not be compared directly. They must be unified into a common reference system before comparison. With a reasonable assumption that the dominant motion vector of a landslide is downward along the slope surface, we chose the direction of slope gradient as the common reference to facilitate inter-stack comparison. Then all the LOS velocities were projected onto this direction to obtain down-slope velocities using the following equation:

$$V_{slope} = \frac{V_{LOS}}{\cos\theta} \quad (1)$$

where V_{LOS} and V_{slope} represent mean deformation velocities along LOS and down-slope respectively, θ is the intersection angle between the two vectors, *i.e.*, LOS direction and slope surface. After such a conversion, down-slope velocities from multiple data stacks could be compared with each other. In fact, this strategy has been adopted in a few studies recently [23,24].

As V_{LOS} obtained by PS-InSAR is actually a relative measurement with respect to the average deformation velocity across the study area, a calibration operation must be done to offset them to the same reference point before doing the above projection. Location of the reference point is shown in Figure 4(c).

Figure 5 shows the down-slope velocities at PS points for the three data stacks. Negative values of V_{slope} stand for a downward motion of the landslide body along the slope surface. It should be noted that the V_{slope} value depends on $cos\,\theta$. In order to avoid anomalous solutions, a minimum absolute value of $cos\,\theta$ is fixed as 0.3 for this study area and those PS points with $cos\,\theta < 0.3$ are discarded in the following assessment of V_{slope} [24]. Again, we can see that the active deformation zone of Huangtupo landslide near the old town in the eastern part is clearly identified by all of the three stacks, as indicated by the yellow circle in Figure 5. In order to carry out inter-stack comparison within this zone, we manually identified nine positions where PS points extracted from the three stacks were spatially close enough to each other to be considered as the same ground target. Then the differences of down-slope velocities at each position among the three stacks were obtained and statistics were derived.

Figure 5. Down-slope mean deformation velocities at PS points for the three Synthetic-Aperture Radar interferometry (InSAR) data stacks: (**a**) Advanced Land Observing Satellite (ALOS) Phased Array L-band Synthetic Aperture Radar (PALSAR), (**b**) Environmental Satellite (ENVISAT) Advanced Synthetic Aperture Radar (ASAR) ascending, and (**c**) ENVISAT ASAR descending.

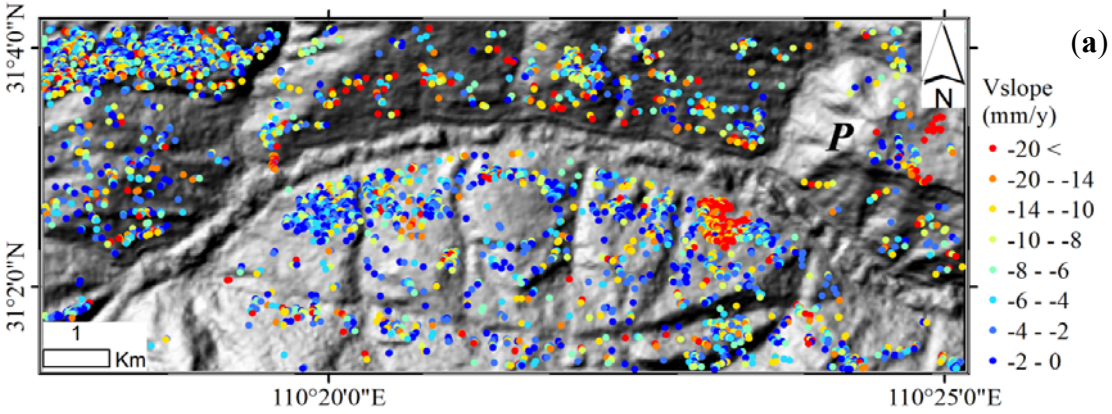

Figure 5. *Cont.*

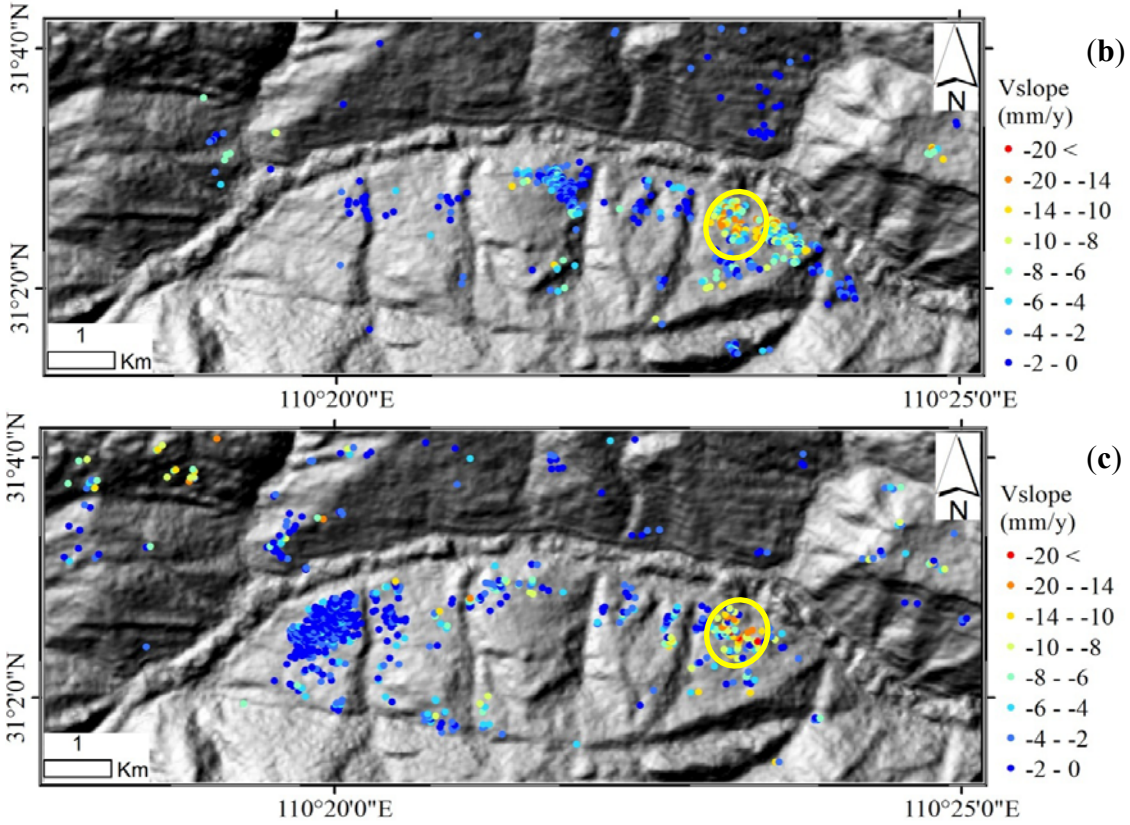

The results show that the smallest root-mean-squared difference (RMSD) of 7.0 mm/yr is attained between the two ENVISAT ASAR stacks. A slightly larger RMSD of 8.6 mm/yr between the two ascending stacks is achieved, while the largest RMSD of 11.9 mm/yr was found to be between the ALOS PALSAR stack and the ENVISAT ASAR descending stack. Nevertheless, such differences are still acceptable for landslide deformation monitoring in the Three Gorges, because in our test area the quantity of landslide motion is usually at a scale of cm that is larger than ground subsidence in urban areas.

In order to further demonstrate the reliability of above PS-InSAR results, we chose a PS point from the deformation zone of Huangtupo landslide and plotted its time-series movements along down-slope direction with respect to the date of slave images in Figure 6. The temporal variation of reservoir water level at the Three Gorges Dam was also illustrated in Figure 6. We can see that the two time series show close correlation with each other during the two periods before and after the first tentative impoundment to the highest water level in late 2008 respectively. For example, when the water level decreased from 173 m in October 2008 to 145 m in July 2009, a significant down-slope deformation of about 14 cm occurred over the period but with a time lag. Following that period, an up-slope deformation of about 5 cm appeared along with the water level rising from 145 m to 155 m. Such a temporal evolution pattern agrees well with the results obtained by Liao *et al*. [25] and Liu *et al.* [12]. However, it should be noted that in those two articles the LOS deformations were used for time-series plotting, while in our study the downslope deformation with a larger fluctuation range was used instead.

Figure 6. Time series of deformation at point P along down-slope direction from Advanced Land Observing Satellite (ALOS) Phased Array L-band Synthetic Aperture Radar (PALSAR) data and water level in Three Gorges Reservoir. The location of point *P* is shown in Figure 5(a).

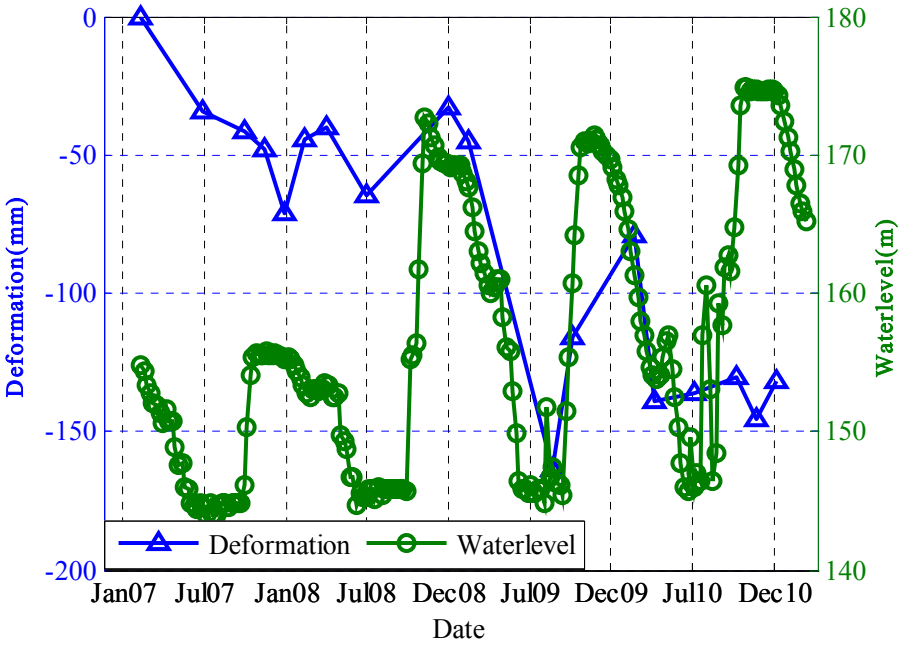

5. Discussion

The landslide deformation in Badong area is analyzed in four aspects of the experimental results, *i.e.*, coherence images, phase interferograms, PS distributions and mean deformation velocity of PS. Three InSAR datasets acquired by ENVISAT ASAR and ALOS PALSAR from different orbits during the period from 2006 to 2011 were used as test data.

The stack of 22 ALOS PALSAR images show the highest coherence because the L-band data can penetrate deeper into the vegetated area. The two ENVISAT ASAR datasets from one ascending and one descending orbit provide high similarity of stable InSAR reflectors only in bare surface areas with little vegetation. Such characteristics cause the low coherence and low density of PS point in the area of rough terrain.

In summary, the experimental results indicate that D-InSAR and PS-InSAR techniques can be used to observe displacement areas in Badong. The InSAR data quality in repeat-pass interferometry can be evaluated using coherence. Coherence in vegetated area is not only related with time interval and normal baseline of data pair but also depends on radar wavelength. Moreover, only the differential interferograms with small normal baselines can provide useful results for rough identification of surface motion. In the case of Badong, with steep topography and dense vegetation, the dissimilar system configurations of each dataset greatly impact the number and spatial distribution of PS points. The system of longer wavelength is more coherent and could usually produce a larger number of PS points.

The two areas of large displacement in Badong are monitored by the three SAR datasets for landslide assessment. The mean deformation velocities in the areas are approximately −14 to −50 mm/y estimated using PS-InSAR technique. The two datasets from ascending orbits can only detect a large displacement

area, *i.e.*, zone of Huangtupo landslide. On the other hand, using the ENVISAT ASAR data acquired from a descending stack two high displacement areas can be identified. Using satellite acquisitions from both ascending and descending orbits, it is possible to overcome the problem of incompleteness in identification of potential landslide risk using just one data stack.

6. Conclusion

In this study, we detected some significant deformations in Badong using the Differential Synthetic-Aperture Radar Interferometry (D-InSAR) technique. However, the deformation detection with this technique is effective only for those data pairs with relatively short time intervals and small normal baselines. Thus, this technique is difficult to be applied for long-term monitoring. Using Persistent Scatterer Interferometry (PS-InSAR), limitations due to geometrical and temporal decorrelations, as well as atmospheric disturbances, can be overcome, and time series monitoring are implemented. Two significant deformation areas in Badong are detected by using PS-InSAR technique.

Furthermore, we can estimate surface deformation trends in the Badong area from the three InSAR data stacks. The unique characteristics of each InSAR stack brought dissimilar distribution patterns of PS points. Joint analysis of SAR datasets of different orbit directions may mitigate the problem of incompleteness in identification of deformation from only one data stack. In this way the reliability and accuracy of deformation monitoring can be improved in areas with complex topography and vulnerable geological conditions. Finally, cross-validation is carried out among the PS-InSAR results from the three data stacks by projection of LOS velocity onto down-slope direction for unification.

Acknowledgments

The anonymous reviewers are appreciated for their helpful comments and suggestions to improve the quality of this paper. The research work in this article was financially supported by the National Key Basic Research Program of China (Grant No.2013CB733205), the National Natural Science Foundation of China (Grant No.41174120, 41271457 and 41021061), and the Major Research Program of the Three Gorges Region Geologic Disaster Protection (Grant No.SXKY3-6-4). The ENVISAT ASAR datasets were provided by ESA through the Dragon-3 program (id 10569). The ALOS PALSAR datasets were provided by JAXA under the ALOS RA3 scientific research projects (PI520 and PI547).

Conflict of Interest

The authors declare no conflict of interest.

References

1. Rosen, P.A.; Hensley, S.; Joughin, I.R.; Li, F.K.; Madsen, S.N.; Rodriguez, E.; Goldstein, R.M. Synthetic aperture radar interferometry. *Proc. IEEE* **2000**, *88*, 333–382.

2. Li, T.; Liu, J.; Liao, M. Monitoring City Subsidence by D-InSAR in Tianjin Area. In Proceedings of IEEE International Geoscience and Remote Sensing Symposium, Anchorage, AK, USA, 20–24 September 2004.
3. Nagler, T.; Rott, H.; Kamelger, A. Analysis of Landslides in Alpine Areas by Means of SAR Interferometry. In Proceedings of IEEE International Geoscience and Remote Sensing Symposium, Toronto, ON, Canada, 24–28 June 2002.
4. Chini, M.; Atzori, S.; Trasatti, E.; Bignami, C.; Kyriakopoulos, C.; Tolomei, C.; Stramondo, S. The May 12, 2008, (Mw 7.9) Sichuan earthquake (China): multiframe ALOS-PALSAR DInSAR analysis of coseismic deformation. *IEEE Geosci. Remote Sens. Lett.* **2010**, *7*, 266–270.
5. Jiang, K.; Wang, C.; Zhang, H.; Chen, W.; Zhang, B.; Tang, Y.; Wu, F. Damage Analysis of 2008 Wenchuan Earthquake Using SAR Images. In Proceedings of IEEE International Geoscience and Remote Sensing Symposium, Cape Town, South Africa, 12–17 July 2009.
6. Perissin, D.; Wang, T. Time-series InSAR applications over urban areas in China. *IEEE J-STARS* **2011**, *4*, 92–100.
7. Ferretti, A.; Prati, C.; Rocca, F. Permanent scatterers in SAR interferometry. *IEEE Trans. Geosci. Remote Sens.* **2001**, *39*, 8–20.
8. Zhang, Y.; Gong, H.; Li, X.; Liu, T.; Yang, W.; Chen, B.; Li, A.; Su, Y. InSAR Analysis of Land Subsidence Caused by Ground Water Exploitation in Changping, Beijing, China. In Proceedings of IEEE International Geoscience and Remote Sensing Symposium, Boston, MA, USA, 8–11 July 2008.
9. Colesanti, C.; Wasowski, J. Investigating landslides with space-borne Synthetic Aperture Radar (SAR) interferometry. *Eng. Geol.* **2006**, *88*, 173–199.
10. Holbling, D.; Fureder, P.; Antolini, F.; Cigna, F.; Casagli, N.; Lang, S. A semi-automated object-based approach for landslide detection validated by persistent scatterers interferometry measures and landslides inventories. *Remote Sens.* **2012**, *4*, 1310–1336.
11. Bovenga, F.; Wasowski, J.; Nitti, D.O.; Nutricato, R.; Chiaradia, M.T. Using COSMO/SkyMed X-band and ENVISAT C-band SAR interferometry for landslides analysis. *Remote Sens. Environ.* **2012**, *119*, 272–285.
12. Liu, P.; Li, Z.; Hoey, T.; Kincal, C.; Zhang, J.; Zeng, Q.; Muller, J. Using advanced InSAR time series techniques to monitor landslide movements in Badong of the Three Gorges region, China. *Int. J. Appl. Earth Obs. Geoinf.* **2013**, *21*, 253–264.
13. Hooper, A.; Zebker, H.; Segall, P.; Kampes, B. A new method for measuring deformation on volcanoes and other natural terrains using InSAR persistent scatterers. *Geophys. Res. Lett.* **2004**, *31*, L23611.
14. Zhang, R.; Liu, G.; Yu, B.; Li, T.; Jia, H. Multi-Platform Persistent Scatterer SAR Interferometry Time Series Analyzing. In Proceedings of Second International Workshop on Earth Observation and Remote Sensing Applications, Shanghai, China, 8–11 June 2012.
15. Ye, R.; Niu, R.; Zhao, Y.; Jiang, Q.; Wu, T.; Deng, Q. Integration of LIDAR Data and Geological Maps for Landslide Hazard Assessment in the Three Gorges Reservoir Area, China. In Proceedings of IEEE International Conference on Geoinformatics, Beijing, China, 18–20 June 2010.

16. Wu, S.; Shi, L.; Wang, R.; Tan, C.; Hu, D.; Mei, Y.; Xu, R. Zonation of the landslide hazards in the forereservoir region of the Three Gorges Project on the Yangtze River. *Eng. Geol.* **2001**, *59*, 51–58.
17. Wu, S.; Wang, H.; Han, J.; Shi, J.; Shi, L.; Zhang, Y. The Application of Fractal Dimensions of Landslide Boundary Trace for Evaluation of Slope Instability. In *Landslide Disaster Mitigation in Three Gorges Reservoir, China*; Springer: Berlin/Heidelberg, Germany, 2009; pp. 465–474.
18. Liu, J.G.; Mason, P.J.; Clerici, N.; Chen, S.; Davis, A.M. Landslide Hazard Assessment in the Three Gorges Area of the Yangtze River Using ASTER Imagery. In Proceedings of IEEE International Geoscience and Remote Sensing Symposium, Toulouse, France, 21–25 July 2003.
19. Xia, Y.; Kaufmann, H.; Guo, X. Differential SAR Interferometry Using Corner Reflectors. In Proceedings of IEEE International Geoscience and Remote Sensing Symposium, Toronto, ON, Canada, 24–28 June 2002.
20. Wang, T.; Perissin, D.; Liao, M.; Rocca, F. Deformation Monitoring by Long Term D-InSAR Analysis in Three Gorges Area, China. In Proceedings of IEEE International Geoscience and Remote Sensing Symposium, Boston, MA, USA, 8–11 July 2008.
21. Ferretti, A.; Savio, G.; Barzaghi, R.; Borghi, A.; Musazzi, S.; Novali, F.; Prati, C.; Rocca, F. Submillimeter accuracy of InSAR time series: Experimental validation. *IEEE Trans. Geosci. Remote Sens.* **2007**, *45*, 1142–1153.
22. Tantianuparp, P.; Balz, T.; Wang, T.; Jiang, H.; Zhang, L.; Liao, M.; Analyzing the Topographic Influence for the PS-INSAR Processing in the Three Gorges Region. In Proceedings of IEEE International Geoscience and Remote Sensing Symposium, Munich, Germany, 22–27 July 2012.
23. Cascini, L.; Fornaro, G.; Peduto, D. Advanced low- and full-resolution DInSAR map generation for slow-moving landslide analysis at different scales. *Eng. Geol.* **2010**, *112*, 29–42.
24. Herrera, G.; Gutiérrez, F.; García-Davalillo, J.C.; Guerrero, J.; Notti, D.; Galve, J.P.; Fernández-Merodo, J.A.; Cooksley, G. Multi-sensor advanced DInSAR monitoring of very slow landslides: The Tena Valley case study (Central Spanish Pyrenees). *Remote Sens. Environ.* **2013**, *128*, 31–43.
25. Liao, M.; Tang, J.; Wang, T.; Balz, T.; Zhang, L. Landslide monitoring with high-resolution SAR data in the Three Gorges region. *Sci. China Earth Sci.* **2012**, *55*, 590–601.